

Available online at www.sciencedirect.com

jmr&t
Journal of Materials Research and Technology
www.jmrt.com.br



Original Article

Corrosion behaviour of Ti6Al4V ELI nanotubes for biomedical applications



Joan Lario^{a,*}, Mauricio Viera^a, Ángel Vicente^a, A. Igual^b, Vicente Amigó^a

^a Universitat Politècnica De València, Instituto De Tecnología De Materiales, Camino de Vera s/n, 5E Building, 46022 Valencia, Spain

^b Ecole Polytechnique Fédérale de Lausanne, Tribology and Interface Chemistry Group, EPFL SCI STI SM, Station 12, CH-1015 Lausanne, Switzerland

ARTICLE INFO

Article history:

Received 4 August 2019

Accepted 7 September 2019

Available online 4 October 2019

Keywords:

Ti6Al4V ELI

Nanotubes

Corrosion

EIS

Surface treatments

ABSTRACT

Surfaces engineering on titanium biomedical alloys aiming for improving bone regeneration, healing periods and increasing lifetime needs for a fundamental understanding of the electrochemical reactions occurring at the interface biomaterial/human fluid. There, electrochemical corrosion plays an important role in implant-tissue interaction. The aim of this study is to investigate the effect of different TiO₂ surfaces and nanotubes on a Ti6Al4V ELI in their electrochemical corrosion resistance by different electrochemical techniques (open circuit potential, electrochemical impedance spectroscopy, and potentiodynamic polarization). The electrochemical behaviour of native, anodized, nanotubular and annealed nanotubular surfaces were investigated in 1 M NaCl solution. The nanotubular topography was obtained by electrochemical oxidation and the annealing treatment allowed at changing the crystalline structure of the oxides. The nanotube morphology, chemical composition, and structure was studied by Field Emission Scanning Electron Microscopy, Energy Dispersive Spectroscopy, X-ray diffraction and Transmission Electron Microscopy respectively. The results show that the anodic oxidation treatment creates a nanotubular topography that increases the surface area and changes the surface chemical composition. The electrochemical corrosion resistance decreased on the as-formed TiO₂ tubes compared to the native oxide layer, due to higher surface area and amorphous crystal structure of the passive film. After annealing treatment, the fluoride ions are eliminated, and nanotubular resistance is enhanced through anatase stabilization.

© 2019 The Authors. Published by Elsevier B.V. This is an open access article under the CC BY-NC-ND license (<http://creativecommons.org/licenses/by-nc-nd/4.0/>).

1. Introduction

The main objective of titanium prosthesis is to alleviate pain, recover mobility and functionality, and improve patient quality of life. The modification of surface roughness in the micro or nanoscale increases the implant surface area, enhances the

* Corresponding author.

E-mail: joalafe@posgrado.upv.com (J. Lario).

<https://doi.org/10.1016/j.jmrt.2019.09.023>

2238-7854/© 2019 The Authors. Published by Elsevier B.V. This is an open access article under the CC BY-NC-ND license (<http://creativecommons.org/licenses/by-nc-nd/4.0/>).

protein absorption and improves the cell proliferation rate, reducing the bone regeneration periods [1]. Indeed, one of the most common commercial modification of titanium surfaces are obtained by alumina or hydroxyapatite grit-blasting followed by acid-etching (e.g. SLA from Straumann AG and Osseotite/T3 from ZimmerBiomet) [2]. The development of new surface treatments to improve the long-term performance of implants and to reduce recovery periods in patients have recently attracted the interest of many researchers [3–8].

The biocompatibility of titanium implants depends on the physicochemical and electrochemical properties of the oxide film [8–11]. The native oxide layer, which is 1–5 nm thick, spontaneously formed on the metal surface hinders the ion release; thus the oxide layer is considered as the responsible of the high biocompatibility of titanium alloys [12]. The material composition, crystal structure and surface area influence the oxide layer electrochemical properties [13–16]. These parameters can be modified by different surface treatments such as the anodic oxidation process or by applying heat treatments after anodization [17–20].

Titanium alloys are also susceptible to develop thick oxide layers on their surfaces when subjected to an anodic oxidation process [21]. The electrochemical oxidation process with fluoride ions has drawn researchers interest due to the possibility to obtain a titania nanotubular topography on titanium alloys [22–25]. This surface treatment improves osteoblast proliferation compared with the usually applied commercial surface treatments [26–29]. As-formed titania nanotubes contain amorphous crystal phases, but using appropriate annealing treatment can induce amorphous to anatase/rutile phase transformation [6,20].

Generally, the titanium surface degradation occurs due to the interfacial reaction between the passive film and the surrounding environment. The elevated surface area and amorphous structure of titanium dioxide nanotubular surfaces may decrease the titanium alloy corrosion performance. High corrosion resistance of surface treatments is required to reduce the release of metallic ions into the body, which can be harmful to the organism. In-vitro electrochemical characterization constitutes one of the first steps to evaluate new surface treatments for biomedical applications.

The purpose of the present study is to evaluate the effect of nanotopography on the corrosion resistance of the Ti6Al4V ELI alloy. Furthermore, the effect of annealing treatment applied on the nanotubular surface is also discussed.

2. Experimental procedure

2.1. Materials and surface characterization

Ti6Al4V ELI alloy was provided by Allegheny Technologies (ATI Metals, Pittsburgh, PA, USA). The titanium alloy bar was machined to produce disk samples (12.7 mm in diameter, 4 mm thick). Optical metallography analysis was carried out to identify morphology, homogeneity, and distribution of the titanium alloy constituent phases (LV100 Nikon, Tokyo, Japan). The samples were etched with a Kroll reagent in order to reveal the phases domains on the titanium alloy. The surface morphology after electrochemical anodization was character-

ized by Field Emission Scanning Electron Microscopy (FESEM ULTRA 55) (ZEISS, Oberkochen, Germany). Elemental analysis for the different surface treatments were carried out using Energy Dispersive Spectroscopy (EDS) from Oxford Instruments Ltd. (Abingdon-on-Thames, UK).

2.2. Anodic oxidation

Test disks were wet-ground with different silicon carbide paper before the anodizing process. Two anodic oxidation processes were carried out. The first one the electrolyte employed was a solution 1 M H_3PO_4 , applying a constant voltage of 15 V for 15 s. The second anodizing process a 0.8%wt. of NaF was added into 1 M H_3PO_4 solution, and anodizing time was increase till 45 min. The electrochemical treatment to modify the oxide layer present at the alloys surface a two-electrode cell was employed, titanium disk as anode and a 316 L stainless steel as cathode, in a DC Power Supply SM 400-AR-8 (Delta Elektronica, Zierikzee, The Netherlands). After the anodic oxidation process samples were rinsed with sodium bicarbonate solution followed with distilled water to neutralize the electrolyte.

2.3. Annealing treatment

The annealing treatment applied on the nanotubular surfaces was done to evaluate the influence on the corrosion resistance. It was done in an HVT 15/75/450 vacuum sintering furnace (Carbolite Gero Ltd., Parson, United Kingdom) at $<10^{-4}$ mbars heated till 320 °C at 5 °C/min held for 30 min and furnace cooled at 10 °C/min to favor the thermal decomposition of $[TiF_6]^{2-}$ complex.

Additional to the annealing treatment carried out for electrochemical analysis, a second annealing treatment was performed on the as-formed nanotubes. The aim for this heat treatment was to investigate the effect of increasing the time and maximum temperature on the TiO_2 crystal phase stability.

2.4. Electrochemical measurements

The electrochemical behaviour of the non-treated (native oxide layer) and surface-modified titanium alloys (nanotubular and anodized) was investigated using a standard three-electrode cell: the titanium samples as the working electrode (0.78 cm²), a Pt foil as the counter electrode and a Ag/AgCl (3M KCl) as the reference electrode. The titanium samples were immersed in 1 M NaCl solution for 1 h to stabilize the OCP to a steady-state potential (E_{OCP}). Electrochemical Impedance Spectroscopy (EIS) was carried out at the stabilized OCP. The amplitude of the applied alternating sinusoidal potential was ± 10 mV at the E_{OCP} within the frequency range between 5 mHz to 100 kHz. The acquired EIS data were curve fitted using an electrical equivalent circuit (EEC) with the ZView programme (version 3.5a from Scribner Associates Inc., Southern Pines, NC, USA). Quality of fit was checked by the χ^2 value. After the EIS measurements, potentiodynamic polarization curves were carried out at a scan rate of 2 mV/s within the potential range from OCP to 3.5 V. From them, the corrosion potential (E_{corr}), corrosion current density (i_{corr}) and passive current (i_{pass}) were obtained.

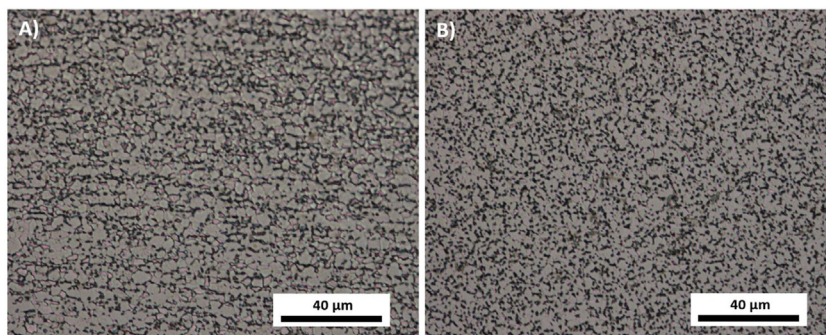


Fig. 1 – Optical images of the Ti6Al4V ELI microstructure. A) Longitudinal section. B) Cross section.

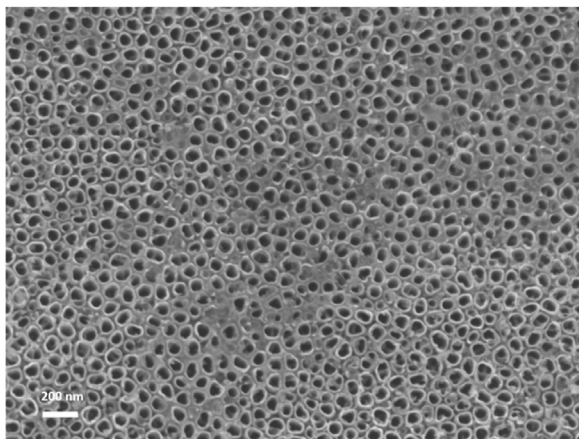


Fig. 2 – Nanotubular topography on Ti6Al4V ELI after anodic oxidation process at 15 V.

2.5. Nanotubular crystal phase characterization

The crystal structure of nanotubular surfaces was determined using X-ray diffraction instrument (D8 AXS, Bruker) with $\text{CuK}\alpha$ radiation, operating at 40 kV and 40 mA (Bruker, Massachusetts, USA). A detailed scan was done over the 2θ range of 20° – 120° with a step size of 0.03° . For transmission electron microscopy (TEM) and selected area electron diffraction (SAED) investigation nanotubes were delaminated directly onto square mesh copper with ultra-thin carbon substrate coating by using a scapel. The delaminated nanotubes were observed with JEM 2100F (JEOL Ltd., Tokyo, Japan) electron microscope at an accelerating voltage of 200 kV.

3. Results

3.1. Surface characterization

The cold work process performed on the melt and forge Ti6Al4V ELI bar results in a micrometre non-equiaxial grain with a fine dispersion of the alpha and beta phases (Fig. 1). The microstructure is a relevant property that influences the mechanical properties and corrosion resistance of titanium alloys [30–32].

Fig. 2 shows the nanotubular layer obtained from FESEM image after the electrochemical process. The nanotubes have a diameter of approximately of 64 nm and inter-tube distance around 9 nm. The chemical composition of the material after the different surface treatments obtained by EDS are summarized in Table 1. The quantity of oxygen and fluorine measured with EDS increases anodic oxidation process. After annealing at 320°C the fluorine weight percentage decreased from 5%wt to 0.5%wt.

3.2. Microstructural characterization

The XRD patterns for native oxide layer, nanotubes, and annealed nanotubes are shown in Fig. 3. The XRD pattern of the as-formed nanotubular oxide layer shows the incorporation fluoride ions on the nanotubular topography, represented on higher relative intensity peak found at 45° compared with the native oxide layer. The increase in relative intensity peak is related to TiF_6^{2-} complex formation [26]. On the other hand, after annealing treatment, the 45° relative intensity peak decrease due to TiF_6^{2-} the thermal decomposition, corroborating EDS results. The annealing treatment also stabilizes the titanium dioxide anatase crystal phase, reflected in higher relative intensity values located at 41° and 75° for annealed samples, compared with native or as-formed nanotubular oxide layers.

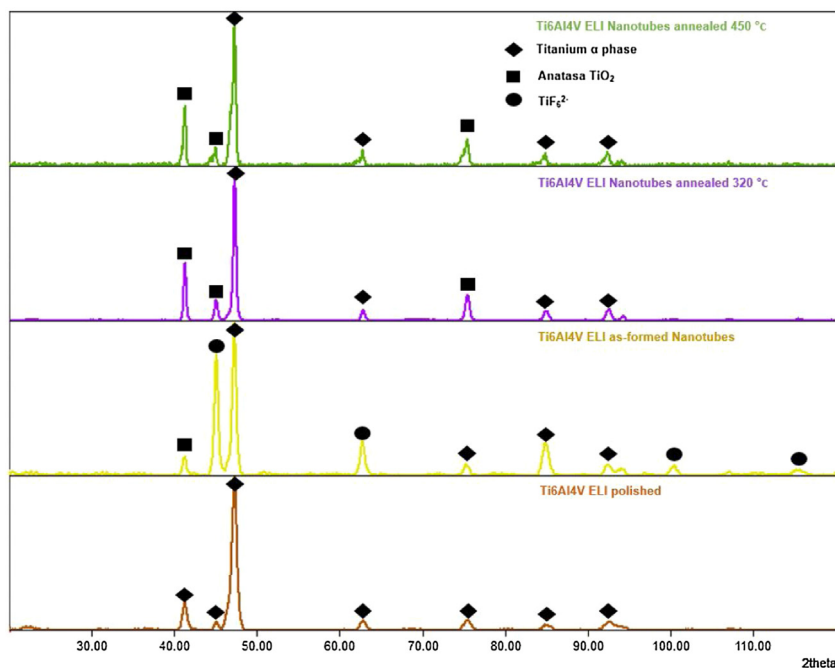
Fig. 4 shows high-resolution transmission electron microscope (HRTEM) images and selected area diffraction patterns for the delaminated nanotubes. The first images (bright field (BF) HRTEM, Fig. 4A, or SAED images, Fig. 4B) correspond to the nanotubes annealed at 320°C for 30 min. in vacuum, where no crystal planes or patterns were found. The annealing treatment at 450°C and 120 min was able to stabilize the TiO_2 crystal phase, as it can be observed with the presence of crystal planes in BF HRTEM and SAED images shown in Fig. 4D.

3.3. Corrosion behaviour

Open circuit potential evolution with time of the four Ti6Al4V ELI surface treatments was recorded and it is represented in Fig. 5. The OCP values for the different surface treatments keep shifting positively during immersion time until steady state is achieved. The polished samples showed the lowest OCP potential (-0.26 V) and achieved a stabilization rate of $1 \times 10^{-9}\text{ dE/dt}$ after longer period. Higher OCP variation is observed after the

Table 1 – Surface chemical composition of the studied samples from Energy Dispersive Spectroscopy (EDS).

Samples	Ti (wt%)	O (wt%)	F (wt%)	Al (wt%)	V (wt%)
Polished	90 ± 1	–	–	4 ± 0.2	6.7 ± 0.2
Nanotubes	66 ± 2	22 ± 1.5	5 ± 0.5	4.7 ± 0.2	2.9 ± 0.8
Annealed Nanotubes	70 ± 2	21 ± 1.7	0.5 ± 0.2	3.7 ± 0.2	2.7 ± 0.2

**Fig. 3 – XRD patterns of different surface treatment for Ti6Al4V ELI.**

anodic oxidation process; suggesting that a protective oxide film is formed. Such a phenomenon is related to oxide layer changes (morphology, chemical composition and morphology). The anodized surfaces are one of the fastest samples to stabilize the OCP, due to 20 nm thick and compact oxide layer formation [33]. While nanotubular samples, that present higher specific area per volume and a thicker oxide layer, requires more time to achieve stability (Fig. 5). Finally, the annealed nanotubes were the surface treatment that faster stabilized the OCP.

Fig. 6a and b shows the Nyquist spectra and the Bode plots respectively of the different titanium surface treatments at E_{OCP} . In all cases, a high impedance (around $10^7 \Omega \text{ cm}^2$) at low frequencies are observed, typical from passive material and suggesting high corrosion resistance of all the studied samples. The higher phase angles obtained for the anodized surfaces compared to the polished surface at the high-frequency region is attributed to the oxide film thickening [34]. At medium and low frequency, the phase angles remain roughly constant, proving capacitive behaviour that it is indicative that elevated protectiveness.

A significant variation on the phase angles was observed on the anodized samples compared with the polished samples. These variations are related to the porosity and crystal phase of the oxide layer. The phase angles lower than 80° observed, at low and medium frequencies, were associated with the nanotubular nature of the outer layer. The higher

phase angles in the high-frequency region were attributed to the oxide film thickening of the anodized samples compared to the polished surface. Also, after the annealing treatment of the nanotubular surfaces show higher phase angles compared to the as-formed nanotubes. This increment is related to changes in the TiO_2 crystal structure.

The potentiodynamic polarization results for the polished substrate, and anodized samples are represented in Fig. 7. The average corrosion potentials obtained from these curves were 0.13 V (as-formed nanotubes) < 0.19 V (polished) < 0.42 V (annealed nanotubes) < 1.47 V (anodized). Polished samples show a perfect Tafel behaviour after the corrosion potential and the highest current density values along most of the passive domain (from 0.5 V to 2 V). The anodized or nanotubular samples show a mixed control (activation and mass transport through the oxide film) around their corrosion potential. As appear summarized in Fig. 7, the anodized samples present lower current density values, in the potential range between 800 mV to 3000 mV, that polished sample. This phenomenon is related to the formation of a protective film (compact or porous) at titanium alloy surface that inhibits its corrosion rate. As-formed nanotubular surfaces present a higher surface area and amorphous oxide, compared to the compact oxide layer formed on the anodized or native oxide layer from the polished samples. After the annealing treatment of the nanotubular structure a more stable oxide layer is formed, due to the elimination of fluoride ions on the nanotubes and crys-

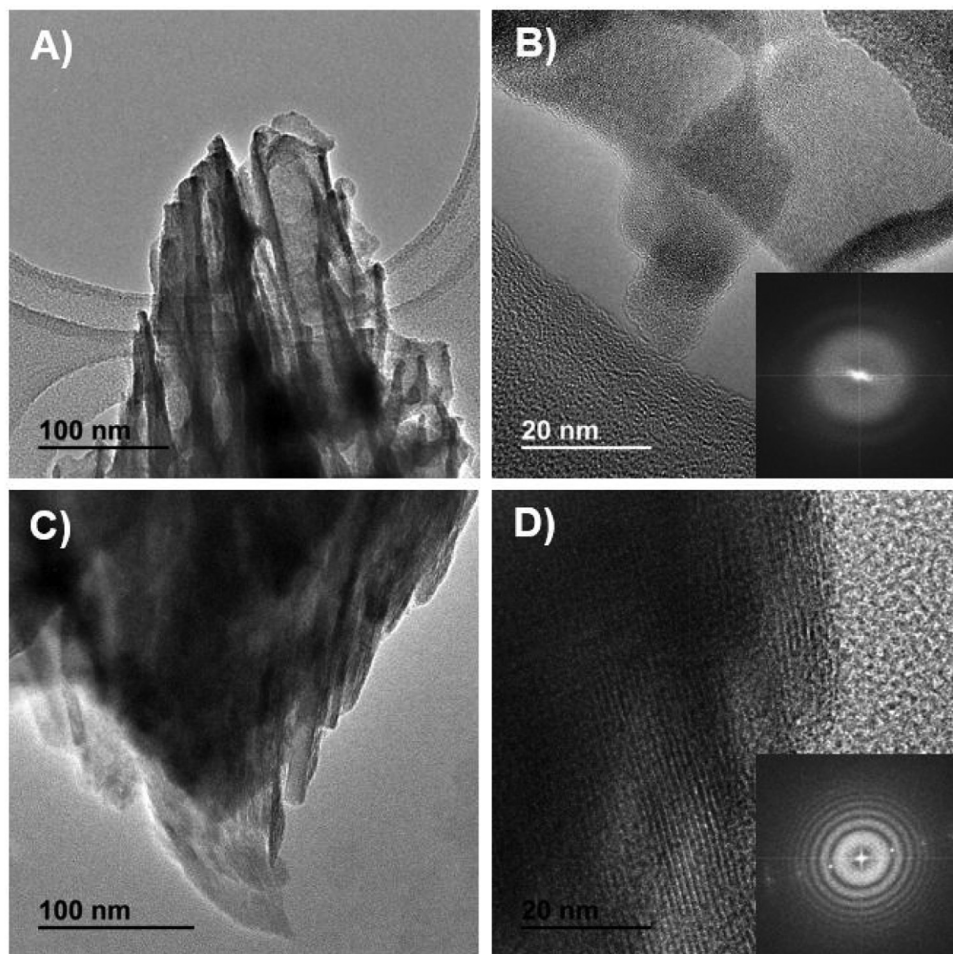


Fig. 4 – Transmission electron micrographs of Ti6Al4V ELI nanotubes. A) Annealed nanotubes at 320 °C. B) HRTEM and SAED images for annealed nanotubes at 320 °C. C) Annealed nanotubes at 450 °C. D) HRTEM and SAED images for annealed nanotubes at 450 °C.

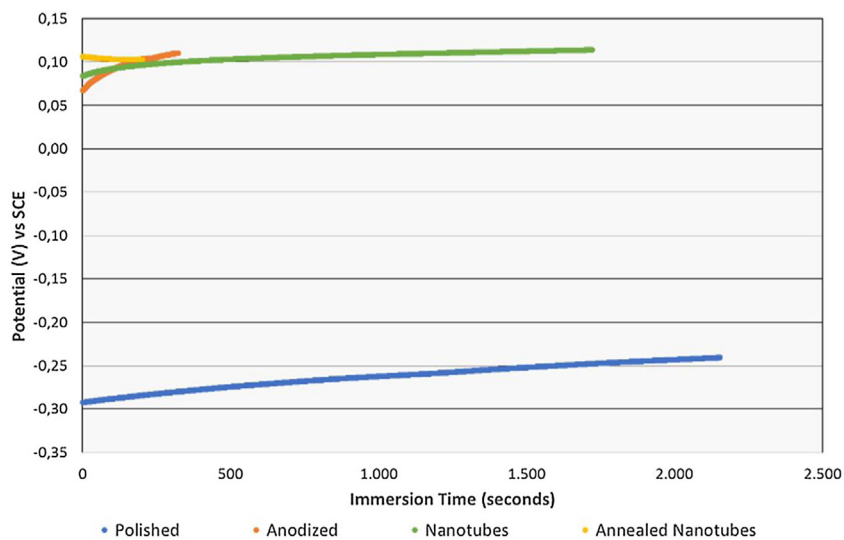


Fig. 5 – Open-circuit potential evolution with time of the four Ti6Al4V ELI surface treatments in 1 M NaCl.

tal phase stabilization, which increase the corrosion potential and reduce ion release (lower current density values). Very low current densities obtained on the nanotubular and anodized

surfaces show a strong passivating behavior (Fig. 7). The calculated corrosion kinetic parameters as corrosion potential (E_{corr}), corrosion current density (I_{corr}), polarization resistance

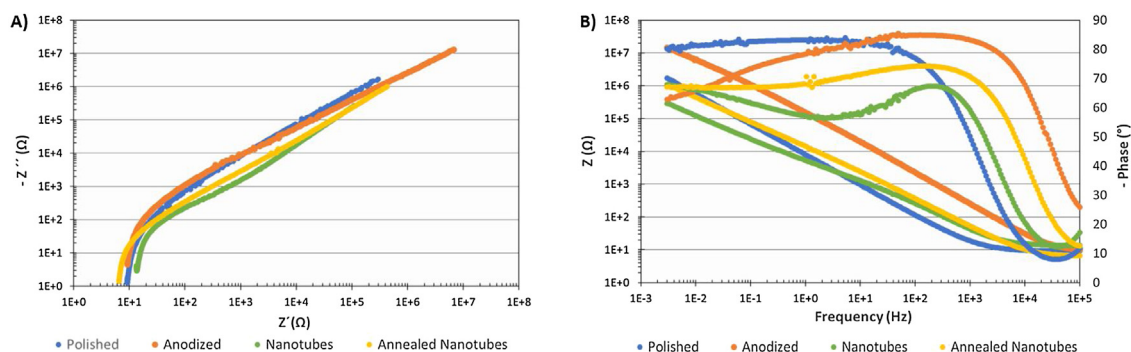


Fig. 6 – Electrochemical impedance spectroscopy measurements of the titanium samples in 1 M NaCl. A) Nyquist Plots. B) Bode plots.

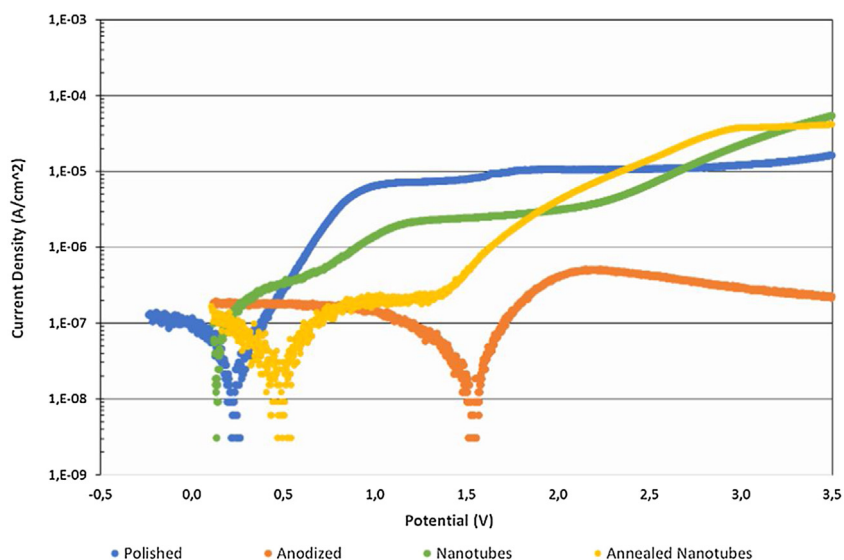


Fig. 7 – Potentiodynamic polarization curves of the titanium samples in 1 M NaCl.

Table 2 – Corrosion parameters from the polarization plots.

Samples	E_{corr} (V)	I_{corr} (A/cm ²)	PR (Ω)	I_p 1 V (A/cm ²)	I_p 2 V (A/cm ²)	I_p 3 V (A/cm ²)
Polished	0.19 ± 0.06	$7.7 \pm 3.0 \times 10^{-8}$	$1.3 \pm 0.6 \times 10^6$	$6.3 \pm 5.9 \times 10^{-6}$	$9.2 \pm 7.2 \times 10^{-5}$	$3.3 \pm 1.2 \times 10^{-5}$
Anodized	1.47 ± 0.13	$1.6 \pm 1.5 \times 10^{-7}$	$2.5 \pm 0.2 \times 10^6$	$3.2 \pm 2.2 \times 10^{-7}$	$8.8 \pm 3.2 \times 10^{-7}$	$6.0 \pm 1.7 \times 10^{-7}$
Nanotubes	0.13 ± 0.01	$9.0 \pm 3.7 \times 10^{-8}$	$2.3 \pm 1.1 \times 10^5$	$3.6 \pm 1.8 \times 10^{-6}$	$7.6 \pm 3.6 \times 10^{-6}$	$3.5 \pm 2.7 \times 10^{-4}$
Annealed Nanotubes	0.43 ± 0.05	$1.4 \pm 1.2 \times 10^{-7}$	$1.8 \pm 1.1 \times 10^6$	$3.5 \pm 0.3 \times 10^{-7}$	$7.6 \pm 0.5 \times 10^{-6}$	$4.6 \pm 2.2 \times 10^{-5}$

(PR) and passive current density (I_p) have been presented in Table 2. The anodized surface displays better corrosion resistance if it shows more positive E_{corr} , higher PR and lower i_{corr} values.

The corrosion current density for polished and nanotubular samples are at least one order of magnitude higher than anodized or annealed nanotubes surfaces. After the annealing treatment, the anodization polarization curve of the nanotubular surface showed a much smaller passivation current density than as formed nanotubular surface. For both nanotubular surfaces (as formed or annealed) the anodic curve (Fig. 7) can be divided into three potential domains. For example, for the annealed nanotubes at the potential domain between $0.5 V_{SCE}$ and $0.8 V_{SCE}$ is featured by a transition stage where the current density increases with the potential due to

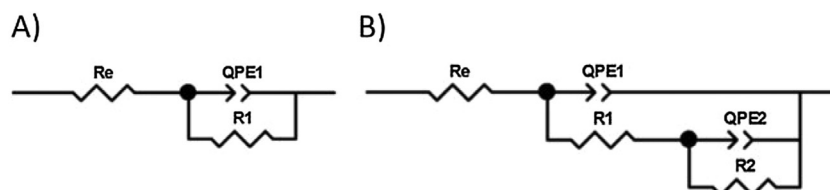
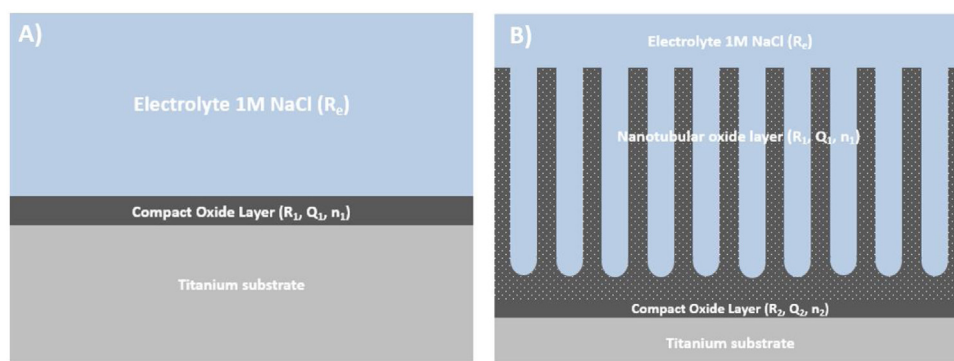
oxidation of Ti_xO_y complex and replacement of the oxide film. The second domain corresponds to the passivation plateau, which ranges $0.8 V_{SCE}$ to $1.4 V_{SCE}$, where the annealed nanotubular surface enters into the stable passivation region, and the current density remains unaltered. The last domain is related to the nanotubular breakdown, which ranges from $1.4 V_{SCE}$ to $3.5 V_{SCE}$. This overpotential applied to the sample produces the collapse of the nanotubular oxide geometry.

4. Discussion

Two equivalent electrical circuits (ECCs) were employed to fit the EIS experimental data (Fig. 8). The native oxide layer on the polished surfaces was simulated with first EEC. The second ECCs was employed to simulate the response of anodic

Table 3 – The electrochemical impedance parameters obtained by fitting an equivalent circuit model for the substrate and nanotube samples.

Samples	R_e ($\Omega \text{ cm}^2$)	R_1 ($\Omega \text{ cm}^2$)	QPE_1 (F cm^2)	n_1	R_2 ($\Omega \text{ cm}^2$)	QPE_2 (F cm^2)	n_2	χ^2
Polished	9.4	3.1×10^7	2.3×10^{-5}	0.92	–	–	–	6×10^{-4}
Anodized	9.1	2.0×10^5	4.5×10^{-7}	0.94	9.8×10^{12}	1.3×10^{-11}	0.58	1×10^{-3}
Nanotubular	12.9	2.6×10^3	2.0×10^{-6}	0.83	2.9×10^8	3.6×10^{-6}	0.67	1×10^{-3}
Annealed Nanotubular	6.1	1.6×10^4	1.5×10^{-6}	0.85	8.5×10^8	1.3×10^{-8}	0.65	2×10^{-3}

**Fig. 8 – Equivalent circuit models. A) Ti6Al4V ELI Polished surfaces. B) Ti6Al4V ELI nanotubes surfaces.****Fig. 9 – Schematic representation of the oxide layer. A) Native oxide layer. B) Nanotubular.**

and nanotubular surfaces. To consider the capacitors non-ideal behaviour the QPE elements were selected to simulate the experimental data. For the polished surfaces (native oxide layer) R_e represents the solution resistance, and R_1 and Q_1 , respectively, represent the resistance and capacitance of the passive oxide layer formed spontaneously on the titanium surface (Fig. 8A). Two-time constants ECC was employed to model the behaviour of the anodic oxidized surfaces (Fig. 8B), in which R_e was the solution resistance, R_1 and QPE_1 were the resistance and constant phase element of the nanotube layer, and R_2 and QPE_2 were the resistance and constant phase element of the inner barrier layer.

Table 3 summarizes the electrochemical parameters employed to fit EIS measurements with the ECCs proposed to simulate oxide layer response. The chi-square values of the 10^{-3} order indicate a good agreement between the experimental and simulated values. These low “n” values of the constant phase elements imply that the nanotube layer for both anodized samples were very leaky, as described by Mohan et al. (2015) in the electrochemical study of TiO_2 nanotubes in Hank's solution [35]. This fact was reflected by the low resistance R_1 values of resistance of the nanotubular surfaces, as-formed $2.6 \times 10^3 \Omega \text{ cm}^2$ and annealed $1.6 \times 10^4 \Omega \text{ cm}^2$. However, the resistance of the inner barrier layer at the bottom of the nanotubes (R_2) was considerably higher, within the range of $10^8 \Omega \text{ cm}^2$, and was higher than the polished bare alloy. The inner layer on the nanotubular surfaces presents lower

resistance than the anodized surface, due to the fact of the higher surface area incorporated by nanotubular topography. This scenario implies elevated corrosion resistance of the nanotubular inner layer.

The presence of a passive oxide film at the bottom of the nanotubes could restrict the movement of the metal ions from the metal surface to the solution and reduce ion release [35]. The relation between the equivalent circuits proposed and the real nanotube morphology observed on FESEM appears represented in Fig. 9. There is a direct relationship between the proposed equivalent electrical circuits (Fig. 8), which simulate the response of the nanotubes, and the real nanotube morphology observed using the FESEM equipment (Fig. 2).

The potentiodynamic results of the present research indicate that the as-formed nanotubular topography reduces the Ti6Al4V ELI corrosion resistance behaviour, and annealing treatment improves the corrosion resistance of the nanotubular oxide layer; this fact is related to fluoride ions reduction and oxides crystal phase formation. The nanotubular topography may be responsible for the penetration of the corrosive anions along with water and increases the corrosion of the metal surface. Alves et al. reported improvement of the corrosion resistance and lower current density after micro-arc oxidation treatment compared with untreated Ti CP2 [36].

Further research into temperature and time of the post heat treatment are required for the stabilization of the oxide layer, to obtain anatase or rutile crystal structure [12,17].

Reducing the effective surface area by applying later surface treatments, as a coating or filling the nanotubes with bioactive agents (hydroxyapatite, calcium phosphate, or antibiotics) may improve nanotube corrosion resistance [37–40]. Further in-vitro and in-vivo researches are required to validate the mentioned processing routes to improve nanotubes surface corrosion resistance.

5. Conclusions

The results of this paper show that anodic oxidation of Ti6Al4V ELI alloy can be successfully used to obtain a nanotube topography on that titanium biomedical alloy. The EIS results showed the formation of a thick oxide layer between the metal/nanotube interface with elevated corrosion resistance. The EEC for nanotubular and anodized surfaces shows that EIS response can be interpreted as an equivalent circuit with two-time constants, where the resistance of the different oxide layers increases as follows: R_1 (nanotube layer) < R_2 (bottom nanotube layer).

The potentiodynamic polarization studies show that the nanotube topography increases the surface area and lowers the corrosion potential compared to the polished bulk alloy. The electrochemical measurements suggested that the annealing treatment after nanotubular oxide formation increases the corrosion resistance with enhanced passivation of the resulting material. The anatase peak was only observed in the XRD pattern of the nanotubular samples after annealing treatment.

Conflicts of interest

The authors declare no conflicts of interest.

Acknowledgments

The authors wish to thank the Spanish Ministry of Economy and Competitiveness for the financial support of Research Project MAT2014-53764-C3-1-R, the Generalitat Valenciana for support through PROMETEO 2016/040, and the European Commission via FEDER funds to purchase equipment for research purposes and the Microscopy Service at the Valencia Polytechnic University. Thanks to Alba Dalmau and Javier Navarro Laboulais from Instituto de Seguridad Industrial y Medio Ambiente, Valencia Polytechnic University for the technical assistance with preparation of the electrochemical tests. Thanks to Irene Llorente and José Antonio Jimenez from CENIM/CSIC for the technical assistance with XRD characterization.

REFERENCES

- [1] Salou L, Hoornaert A, Louarn G, Layrolle P. Enhanced osseointegration of titanium implants with nanostructured surfaces: an experimental study in rabbits. *Acta Biomater* 2015;11:494–502, <http://dx.doi.org/10.1016/j.actbio.2014.10.017>.
- [2] Duraccio D, Mussano F, Giulia M. Biomaterials for dental implants: current and future trends. *J Mater Sci* 2015;50(14):4779–812, <http://dx.doi.org/10.1007/s10853-015-9056-3>.
- [3] Cremasco A, Os WR, Freire MA, Garcia A, Caram R. Electrochemical corrosion behavior of a Ti-35Nb alloy for medical prostheses. *Electrochim Acta* 2008;53:4867–74 <https://doi.org/10.1016/j.electacta.2008.02.011>.
- [4] Huang H, Wu C, Sun Y, Lee T. Improvements in the corrosion resistance and biocompatibility of biomedical Ti-6Al-7Nb alloy using an electrochemical anodization treatment. *Thin Solid Films* 2013;528:157–62, <http://dx.doi.org/10.1016/j.tsf.2012.08.063>.
- [5] Mohan L, Anandan C, Rajendran N. Electrochemical behaviour and bioactivity of self-organized TiO₂ nanotube arrays on Ti-6Al-4V in Hanks' solution for biomedical applications. *Electrochim Acta* 2015;155:411–20, <http://dx.doi.org/10.1016/j.electacta.2014.12.032>.
- [6] Minagar S, Berndt CC, Wang J, Ivanova E, Wen C. A review of the application of anodization for the fabrication of nanotubes on metal implant surfaces. *Acta Biomater* 2012;8(8):2875–88, <http://dx.doi.org/10.1016/j.actbio.2012.04.005>.
- [7] Park IS, Bae TS. The bioactivity of enhanced Ti-32Nb-5Zr alloy with anodic oxidation and cyclic calcification. *Int J Precis Eng Man* 2014;15(8):1595–600, <http://dx.doi.org/10.1007/s12541-014-0508-5>.
- [8] Lario-Femenía J, Amigó-Mata A, Vicente-Escuder Á, Segovia-López F. Desarrollo de las aleaciones de titanio y tratamientos superficiales para incrementar la vida útil de los implantes. *Revista de Metalurgia* 2016;52(4).
- [9] Okazaki Y, Gotoh E. Comparison of metal release from various metallic biomaterials in vitro. *Biomaterials* 2005;26:11–21, <http://dx.doi.org/10.1016/j.biomaterials.2004.02.005>.
- [10] Davis JR. *Handbook of materials for medical devices*. ASM International; 2003, ISBN 0-87170-790-X.
- [11] Gonzalez EG, Mirza-Rosca JC. Study of the corrosion behavior of titanium and some of its alloys for biomedical and dental implant applications. *J. Electroanal Chem* 1999;471: 109–15.
- [12] Demetrescu I, Pirvu C, Mitran V. Effect of nano-topographical features of Ti/TiO₂ electrode surface on cell response and electrochemical stability in artificial saliva. *Bioelectrochemistry* 2010;79(1):122–9, <http://dx.doi.org/10.1016/j.bioelechem.2010.02.001>.
- [13] Bauer S, Pittrof A, Tsuchiya H, Schmuki P. Size-effects in TiO₂ nanotubes: diameter dependent anatase/rutile stabilization. *Electrochim Commun* 2011;13(6):538–41, <http://dx.doi.org/10.1016/j.elecom.2011.03.003>.
- [14] Jang S, Choe H, Ko Y, Brantley WA. Electrochemical characteristics of nanotubes formed on Ti-Nb alloys. *Thin Solid Films* 2009;517(17):5038–43, <http://dx.doi.org/10.1016/j.tsf.2009.03.166>.
- [15] Ossowska A, Sobieszczyk S, Supernak M, Zielinski A. Morphology and properties of nanotubular oxide layer on the “Ti13Zr13Nb” alloy. *Surf Coat Technol* 2014;258:1239–48, <http://dx.doi.org/10.1016/j.surfcoat.2014.06.054>.
- [16] Conde A, De Damborenea J, Arenas MA. Correlation of the nanostructure of the anodic layers fabricated on Ti13Nb13Zr with the electrochemical impedance response. *Corros Sci* 2015;94:61–9, <http://dx.doi.org/10.1016/j.corsci.2015.01.041>.
- [17] Kim E, Jeong Y, Choe H, Brantley WA. Formation of titanium dioxide nanotubes on Ti-30Nb-xTa alloys by anodizing. *Thin Solid Films* 2013;549:141–6, <http://dx.doi.org/10.1016/j.tsf.2013.08.058>.
- [18] Berger S, Hahn R, Roy P, Schmuki. Self-organized TiO₂ nanotubes: factors affecting their morphology and

- properties. *Phys Status Solidi Prop* 2010;2435(10):2424–35, <http://dx.doi.org/10.1002/pssb.201046373>.
- [19] Schmuki JMP. Influence of different fluoride containing electrolytes on the formation of self-organized titania nanotubes by Ti anodization. *J Electroceram* 2006;29–34 <https://doi.org/10.1007/s10832-006-3904-0>.
- [20] Monetta T, Acquesta A, Carangelo A, Bellucci F. Characterization in Hank's solution. *Metals* 2017;7(6):220, <http://dx.doi.org/10.3390/met7060220>.
- [21] Pan J, Thierry D, Leygraft C. Electrochemical impedance spectroscopy study of the passive oxide film on titanium for implant application. *Electrochimica Acta* 1996;41(7-8):1143–1153.
- [22] Mendonça G, Mendonça DBS, Araga FJL. Advancing dental implant surface technology—from micron- to nanotopography. *Biomaterials* 2008;29:3822–35, <http://dx.doi.org/10.1016/j.biomaterials.2008.05.012>.
- [23] Berger S, Albu SP, Schmidt-Stein F, Hildebrand H, Schmuki P, Hammond JS, et al. The origin for tubular growth of TiO₂ nanotubes: a fluoride rich layer between. *Surf Sci* 2011;605(19–20):L57–60, <http://dx.doi.org/10.1016/j.susc.2011.06.019>.
- [24] Ferreira CP, Gonc MC, Caram R, Bertazzoli R, Rodrigues CA. Effects of substrate microstructure on the formation of oriented oxide nanotube arrays on Ti and Ti alloys. *Appl Surf Sci* 2013;226–34, <http://dx.doi.org/10.1016/j.apsusc.2013.08.041>.
- [25] Cai Q, Yang L, Yu Y. Investigations on the self-organized growth of TiO₂ nanotube arrays by anodic oxidization. *Thin Solid Films* 2006;515:1802–6, <http://dx.doi.org/10.1016/j.tsf.2006.06.040>.
- [26] Puckett SD, Peng P, Ciombor DM, Aaron RK, Webster TJ. Nanotextured titanium surfaces for enhancing skin growth on transcutaneous osseointegrated devices. *Acta Biomater* 2010;6(6):2352–62, <http://dx.doi.org/10.1016/j.actbio.2009.12.016>.
- [27] Nelson C, Oshida Y, Henrique J, Lima C, Alberto C. Relationship between surface properties (roughness, wettability and morphology) of titanium and dental implant removal torque. *J Mech Behav Biomed Mater* 2008;1:234–42, <http://dx.doi.org/10.1016/j.jmbbm.2007.12.002>.
- [28] Sista S, Nouri A, Li Y, Wen C, Hodgson PD, Pande G. Cell biological responses of osteoblasts on anodized nanotubular surface of a titanium–zirconium alloy. *J Biomed Mater Res A* 2013;3416–30 <https://doi.org/10.1002/jbm.a.34638>.
- [29] Brammer KS, Oh S, Cobb CJ, Bjursten LM, Van Der Heyde H, Jin S. Improved bone-forming functionality on diameter-controlled TiO₂ nanotube surface. *Acta Biomater* 2009;5(8):3215–23, <http://dx.doi.org/10.1016/j.actbio.2009.05.008>.
- [30] Niinomi M. Mechanical properties of biomedical titanium alloys. *Mater Sci Eng: A* 1998;243:231–6.
- [31] Rack HJ, Qazi JI. Titanium alloys for biomedical applications. *Mater Sci Eng: C* 2006;26:1269–77 <https://doi.org/10.1016/j.msec.2005.08.032>.
- [32] Pang H, Estrin Y, Kim H, Lapovok R, Ng HP, Jo J. Available from Deakin research online: mechanical strength and biocompatibility of ultrafine-grained commercial purity titanium. *Biomed Res Int* 2013;2013:1–6, <http://dx.doi.org/10.1155/2013/914764>.
- [33] Van Gils S, Mast P, Stijns E, Terryn H. Colour properties of barrier anodic oxide films on aluminium and titanium studied with total reflectance and spectroscopic ellipsometry. *Surf Coat Technol* 2004;185:303–10 <https://doi.org/10.1016/j.surfcoat.2004.01.021>.
- [34] Saji VS, Cheol H, Brantley WA. An electrochemical study on self-ordered nanoporous and nanotubular oxide on Ti–35Nb–5Ta–7Zr alloy for biomedical applications. *Acta Biomater* 2009;5(6):2303–10, <http://dx.doi.org/10.1016/j.actbio.2009.02.017>.
- [35] Xu W, Lu X, Wang LN, Shi ZM, Lv SM, Qian M, et al. In vitro corrosion resistance and biocompatibility of metal injection molded Ti–12Mo alloy for dental applications. *J Mech Behav Biomed Mater Mech Prop* 2018;88(June):534–47 <https://doi.org/10.1016/j.jmbbm.2018.08.038>.
- [36] Alves AC, Wenger F, Ponthiaux P, Celis J, Pinto AM, Rocha LA. Corrosion mechanisms in titanium oxide-based films produced by anodic treatment. *Electrochim Acta* 2017;234:16–27, <http://dx.doi.org/10.1016/j.electacta.2017.03.011>.
- [37] Chen J, Zhang Z, Ouyang J, Chen X, Xu Z. Bioactivity and osteogenic cell response of TiO₂ nanotubes coupled with nanoscale calcium phosphate via ultrasonification-assisted electrochemical deposition. *Appl Surf Sci* 2014;305:24–32, <http://dx.doi.org/10.1016/j.apsusc.2014.02.148>.
- [38] Bayram C, Erdal E, Karahalilo Z, Baki E. Titania nanotubes with adjustable dimensions for drug reservoir sites and enhanced cell adhesion. *Mater Sci Eng C Mater Biol Appl* 2014;35:100–5 <https://doi.org/10.1016/j.msec.2013.10.033>.
- [39] Yan Y, Zhang X, Huang Y, Ding Q, Pang X. Antibacterial and bioactivity of silver substituted hydroxyapatite/TiO₂ nanotube composite coatings on titanium. *Appl Surf Sci* 2014;314:348–57, <http://dx.doi.org/10.1016/j.apsusc.2014.07.027>.
- [40] Yao C, Webster TJ. Prolonged antibiotic delivery from anodized nanotubular titanium using a co-precipitation drug loading method. *J Biomed Mater Res B Appl Biomater* 2009;(February):587–95 <https://doi.org/10.1002/jbm.b.31433>.